Dear Editor,

Thank you for the decision to accept our manuscript for publication in the *Wind Energy Science* journal, after implementing the improvements suggested by the three reviewers. We have incorporated the majority of their comments, but at the same time we tried to keep the manuscript concise. Below is a list with the most important changes in the document.

- We added vertical profiles of the wind speed and turbulence intensity. Altough the data was measured during a previous measurement campaign, the conditions in and settings of the wind tunnel were identical, such that we can assume that they are valid in our case.

- As suggested by multiple reviewers, we added an uncertainty estimate of the measured lidar line-of-sight wind speeds as a consequence of neglecting the vertical wind speed component. It is mentioned throughout the paper now that there might be a bias and a ,worst-case' estimate is taken into account in the uncertainty analysis as well.

- The ability of the lidars to measure small scale turbulence is explained in a clearer way and it is stressed that the probe length averaging filters out the smallest turbulence scales, compromising the lidars' abilities in that respect. A reviewer pointed out an inconsistency regarding the calculation of the ,cut-off' frequency of the lidar probe length and this has been fixed.

To avoid providing redudant information, we will not repeat the remaining minor changes to the document. These can be found both in the author's responses to the three reviewers, as well as in the marked-up version of the revised manuscript. We hope that this reports our minor revision sufficiently.

Dear Dr. Iungo,

Thank you very much for the critical and in-depth review of our manuscript. It has an overall positive tone, but convincingly addresses some shortcomings of the paper that can be improved to prepare it for publication in the Wind Energy Science journal. Below we will address each of your comments separately.

1. P1 L21: I agree that a wind tunnel provides the great advantage of fixing different flow parameters, such as speed and turbulence intensity. However, I would mention that we should be able to reproduce the wind field variability consequent to the daily cycle of the atmospheric static stability, or mimic a realistic wind rose.

   It is indeed good to mention this drawback of measuring in a wind tunnel. Therefore we added the sentence ,*Please note that one of the shortcomings of measuring in a wind tunnel as opposed to free-field measurements is the ability of simulating the variability of atmospheric stability and a representative wind rose.*'.

2. Sect. 1: I would suggest to expand this introduction to an overview of the most relevant works focused on characterization of wind turbine wakes both for utility scale wind turbines and wind turbine models, which have been performed with different measurement techniques.

   We will add some references that give an overview of the state-of-the-art research being done on wind turbine wake characterisation in both the free-field and in wind tunnel experiments. However, we would like to stress that the objective of this paper is not to do an extensive wake analysis, but it uses wake measurement to provide an interesting and relevant example. This objective will be highlighted more clearly (see your **comment #3**).

3. Sect 1: Add a paragraph to state clearly the aims of this project and the scientific questions you are attempting to address. I guess the main focus will be assessing the capabilities of continuous lidar to measure wind speed and turbulence in a wind tunnel environment.

   You are right. At the end of the introduction, we now added the objective as the sentence ,*The objective is to assess the capabilities of continuous-wave short-range lidar to map wind flows and measure turbulence in a wind tunnel.*'.

4. Sect 1: Add at the end of the section a description of the structure of the paper.

   The structure of the paper will be included at the end of the introduction.

5. P2 L15: Add some references for the wind turbine models and wind energy projects performed at the wind tunnel of PoliMi.

   We believe that there are sufficient references included that are related to both the wind tunnel as well as the model wind turbines. However, they were scattered over the paper and are now repeated in the section you mentioned to have a better consistency for reading.

6. P3 L4: In my opinion, it is a bit too simplistic affirming that we can reproduce an ABL flow in a wind tunnel with spires and turbolators. We would need also to reproduce the temperature profile and typical length scales of the coherent structures. I would say that we can reproduce similar vertical profiles of wind speed and turbulence.

   This is true, the sentence might have exaggerated what the turbulence generators are capable of. We changed it to ,*Typical vertical profiles of wind speed and turbulence can be imitated by the use*

of bricks on the floor that act as roughness and turbulence generators, i.e. spires, placed at the chamber inlet at the left boundary.'.

7. P3 L4: Please add a figure reporting the vertical profile of wind speed and turbulence intensity at the beginning of the turntable.

    Unfortunately we did not execute measurements of the vertical profile during this measurement campaign. However, vertical wind profiles for both wind speed and turbulence were measured during a previous campaign, under identical conditions. These plots are added to the manuscript.

8. P4 L9: I would remove "averaged". Each measurement is a sample corresponding to a given sampling frequency.

    The word *,averaged*' was replaced by *,Doppler spectrum averaged*' to indicate that it is an average over the whole time interval and not just a snap-shot, i.e. the raw signal is actually sampled at 100 MHz, Fourier transformed, and then averaged.

9. P4 L11: Does this lidar have any blind region close to its location?

    There is no blind region close to the lidar, but the optical configuration of the device implies a minimum and maximum possible focus distance. To improve the clarity, the sentence was changed to *,The measurement range is defined by the optical configuration of the device, which enables motor controlled focus distance between about 9 m and 150 m.*'.

10. P4 L19: I think the setup and installation of the lidars in the wind tunnel is not described in detail. It would be interesting for the reader learning about the procedure you applied for the positioning and pointing of the two lidars.

    The procedure for installation and calibration of the lidar has now been extended significantly, in order to have a more complete explanation.

11. P4 L27-28: In my opinion the elevation angle of 3° rather than a contamination from the w velocity, implies an under-estimation of the u- and v-velocities. It will be interesting to quantify error introduced on the horizontal velocities through the uncertainty analysis discussed later in Sect. 3.4.

    Indeed this would be very interesting and other reviewers also mentioned the possible bias in the horizontal wind speed components caused by neglecting the vertical wind component. This will be investigated further by means of uncertainty analysis.

12. P5 L9-13. Did you use the Dantec software for the calibration or do you have your own calibration procedure? In the second case, please provide a description and references.

    The Dantec hot-wire probes were calibrated according to their factory software and manual. The procedure is now explained in detail and a reference is provided.

13. P6 L5-11: It would have been interesting to estimate effects of the probe length on the turbulence statistics by varying the distance between the lidar and the measurement point. Do you have any available data to address this point?

    This would be very interesting indeed. We admit that there is a high dependency on the capability of measuring small-scale turbulence and the probe length, the latter of which increases quadratically with the focus distance. However at this point there is no such data set with which we can assess this issue.

14. P7 L1-3: The characteristics of the incoming velocity field should be reported in Sect. 2.1. Please provide a figure with the vertical profile of velocity, turbulence intensity and integral length scale of the wind tunnel flow.

We now shifted the information about the wind tunnel inflow velocity and turbulence intensity to section 2.1. Also, as we answered to your **comment #7**, we included vertical profiles of wind speed and turbulence from a previous campaign executed under identical conditions and wind tunnel settings.

15. P7 L6-10. It would be more effective to show a chunk of velocity signals for both anemometer and lidar showing the different filtering steps starting from the raw data. Something like Fig. 10, but starting from the initial sampling frequency of the two instruments.

We now included the time series for the 390 Hz u- and v-components as well, before averaging them to 1 Hz time series.

16. Table 1: I would add to the statistics skewness and kurtosis in order to learn more from the statistical behavior of the two signals. Furthermore I would provide statistics for the raw signals (with their sampling frequency), and after 1-s averaging.

The statistical parameters skewness and kurtosis have been added to the table. Also an additional table with the statistics of the 1 Hz averaged time series has been included in addition.

17. Fig. 16. I am not sure if you clarify a significant energy damping for frequencies lower than 28 Hz. I guess you should emphasize that the size of the virtual measurement volume might be much larger than 0.1 m and it's a function of the relative angle between the two-laser beams. A more detailed discussion in this direction may help to better clarify this disagreement with the theoretical expectations.

We clarified the observed behaviour with the text ,*The drop in the slope of the spectrum does not exactly coincide with the 28 Hz frequency mark, because the intrinsic Lorentzian spatial weighting function of a continuous-wave lidar extends beyond the defined bounds of the probe length, therefore also acting as a filter on lower frequencies. The effect of spatial weighting is explained in detail by Sjöholm et al. (2009). Also combining measurements from two lidars that each have a different probe volume causes an even larger effect of averaging out small turbulence scales over a more complex x-shaped volume (see Fig. 4).'.* We believe that this should be sufficient to understand that frequencies lower than 28 Hz are already affected by the volume averaging effect.

Dear Dr. Westergaard,

We appreciate your recommendation for this article to be published. Also thank you for the high level of detail in your review, which we will take into account very seriously. Below we will address each of your comments separately.

1. (major correction) Abstract, p1, l11 and l124 "the larger measurement probe volume" (L11) is directly in conflict with the actual results and the statement in L14 "lidars to accurately measure small scale flow structures". This language should be more precise and accurate to the results. My suggestion would be to accurately describe two things: a) The measurement volume of the LIDARs is 13 to 50 cm, allowing average flow features to be resolved at 0.11D to 0.57D in the far downstream of the three turbine. b) The same volume limitation results in an effective spectral cut-off frequency between 22 and 11 Hz, respectively. This is compared to high resolution HW data.

   It is true that there is a conflict between the lidar's ability to measure small scale flow stuctures on the one hand, and the probe length averaging on the other. Therefore this will be rewritten to provide a better picture of the capabilities. Your concerns regarding the measurement volumes will be addressed in your **comment #13**.

2. (minor), p1 L14 Why is "January 2016" important ? Maybe reformulate.

   We thought it is relevant side information to know when the measurement campaign took place. However, we will move this date to the end of the sentence, where it fits better with regard to its importance.

3. (please elaborate) w-influence, p4, L24-28 w is neglected and deemed insignificant. Never the less, it is measured to be 0.08 m/s and must surely introduce a bias, especially as the vertical projection of the measurement volume is between 0.7 and 2.6 cm (at 3 deg downwards beam orientation, and the two ranges given in fig 5).

   It is a good observation that the vertical wind speed component indeed has a contribution and one could argue that it is not insignificant. Therefore we will extend the uncertainty analysis by incorporating the potential bias in the other two wind speed components that could be caused by neglecting the vertical component.

   (major correction) coordinates of fig 4 Please correct figure 4, so the coordinate system can be understood. Preferably x/D and Y/D, so it is comparable to figure 3

   The only purpose of Figure 4 is actually to sketch the shape of the probe volumes and therefore it is not plotted to any scale. If we use the scale that corresponds to Figure 3, one can barely see the probe volumes, since their dimensions are so much smaller than the focus distances. Therefore we prefer to keep it like this.

4. (major correction) "rated conditions", P6, L15 and L19 (possible other places) "turbines operating under rated conditions" is nonsense. In rated conditions, the pitch of the blades is going positive and all research shows the wake disappears. So, I am pretty sure the author means that the turbine is operating close to maximum wake deficit or maximum Cp. Please be specific: TSR = xx, Pitch = xx, corresponding to an estimate Ct of xx, resulting an estimated wake deficit of xx.

According to our point of view ,*rated conditions*' occur exactly at the one point where the wind turbine first reaches maximum power (also maximum C_p and C_T are theoretically achieved here) and the transition between torque control and pitch control takes place. At this point you indeed have the highest wake deficit. The pitching will occur for wind speeds between the rated wind speed and the cut-out wind speed, in which case the wake is indeed expected to disappear. We will make sure that the reader knows which operational conditions we mean. Therefore we will also provide values for the tip speed ratio, pitch angle and the thrust coefficient of the wind turbine during each part of the experiment.

5. (minor) TI p7, L2 Why not be specific, TI=5.4% (as measured, table 1)

Good point to state the more precise measured turbulence intensity here. This will be adjusted.

6. (major) Table 1 and text on p7 There is an average v and w component. Albeit fairly small it is not really clear if this is a flow feature or probe misalignment ? Please be precise in the language about this.

At the time of writing this response, it is not known where this bias stems from, but it will definitely be investigated and we agree that this has to be addressed in the revised manuscript.

7. (major) Table 1 and text on p7 There is no difference between u' and v' in the table, but yet a very velar difference in figure 8 and 9 scatter ? Either observe or comment on this.

This is indeed an interesting observation which we did not pay much attention to so far. It could just be caused by the scaling of the plot and the range of the wind speeds, but this will be checked.

8. w component Same comment as C3

See the answer on **comment #3**.

9. Error in figure 9 The offset in fig 9 red curve is indicated to be 0.00 – Looks like a mistake. Please check.

In Figure 9 it can be clearly seen that the red regression line crosses the point (0,0), so we could not identify what error you mean. However, it is strange that the slope is quite far off unity. This will be reassessed.

10. (major) effects comparing fig 8/9 to 12/13 P9, L2 "the mentioned effects caused the scatter". I don't think this is accurate. The 3 mentioned effects (p7 L23 to p8 L2) is bias effects. Why would bias effects cause scatter ? The more likely effect is that the small scales are not resolved by the LIDAR.

True, after looking through the reasons given for the scatter, it is concluded that only the first point could indeed be valid. However the other two points could be an explanation for a bias but not for scatter. Also the lidar not being able to resolve small scales is a possible reason. Therefore this part will be slightly rewritten according to this concern.

11. (minor) p9 L3 Delete "most of the very" And "are omitted here" maybe you mean is "averaged away by the large measurement volume"

You are right that this sentence is not very accurate. Therefore we changed it to ,...*since small scale fluctuations are averaged out*.'.

12. (minor) p9 L5 and L6 L5 "in the wind tunnel" should be "in the wind tunnel at 1 Hz". L6 "are estimated that well" should be "at 1 Hz follows the same trend".

It is indeed good to state that this validation is only valid for the 1 Hz measurements. That is why we adapted your suggestion here.

13. (major) p10, L10 The spatial resolution is given to be in the range 0.13 to 0.5 me. This gives 1/2*5.6/0.13 to 1/2 *5.6/0.5, which is 22 Hz to 5.5 Hz temporal resolution.

It is good that you mention this, because there is a slight inconsistency in the manuscript. Namely the probe lengths of 0.13 m and 0.50 m indicated in Figure 5 are valid for focus distances of 10 and 20 m, respectively. However the point measurements were actually executed at a focus distance of 9 m, yielding a probe length of 0.10 m instead of 0.13 m and this translates to the calculated 28 Hz resolution. We will make sure make this consistent throughout the manuscript (in the text and the figures).

It is generally misleading that it is suggested the LIDAR can measure up to 390 Hz.
And the results shows the true range of resolution is 5.5 to 22 Hz. Please correct this throughout the paper.

It is also true that, although the lidar has a sampling rate of 390 Hz, the true resolution of small scales is actually lower. This difference will be described more clearly, also taking into consideration your **comment #1**.

14. (major) figure 16 Introduce 5.5 to 22 Hz. 28 Hz is inaccurate. Also, 5/3 rule should be 5/3 Kolmogorov (since "rule" is not discussed)

Please find the reason for using 28 Hz in **comment #13**. The manuscript will be adjusted to be consistent. Also the Komolgorov rule will be introduced in Figure 16 as you suggest.

15. P11, figure 17/18 It would be prudent to present 22 Hz (or maybe 5.5Hz) filtered data.

In the case of Figure 16, we do not see the need to post-process the data by filtering it to 22 Hz.

16. P11, comments pertaining to figure 18 and w-component It would be prudent to comment that at 3D the w-component is not insignificant and this could have resulted in the "v-component signature", otherwise the reader is left with the impression that this is the turbulence, which is probably not the case.

You raised the valid issue here that the vertical wind speed component (w) might have a significant effect here and even causes the signature in the lateral (v-)component of the flow. This will be discussed in the paper. Also see the answer on your **comment #3**.

17. P11, L16 (minor) "determine local 2D effects", I think you mean "measure a cross section of a wind turbine wake" or something like that

Since this statement was indeed a bit vague, we changed this sentence to '*It (the figure) illustrates that the lidars are capable of determining the two-dimensional flow across a wind turbine wake cross-section.*'.

18. P11, L19 "as well as tip vortex". I don't think that is very clear. It could be turbulence in the shear layer, or the w-component or the shear layer itself.

It will be discussed in the paper that tip vortices cannot be identified with certainty, and the possible other reasons you give will be mentioned and discussed.

19. P11, L21 (major) I tin you either need to reference where the "turbulence in the lower region" has been observed in other studies, or reference shear layer or make it clear that your speculating. Because it could be due to velocity bias in the measurement.

Let it be clear that the 'lower region' refers to the lower part of the plot. The wording might be a bit off here, but we are quite certain that some local effects in the v-component are 'washed away' by the presence of the other overlapping wakes. We will try to state this in a different way and make sure that this is a speculation and not a hard fact.

20. Figure 19 and 20 Introduce 19 a , 19 b and 20 a and 20 b for clarity.

All subfigures will be alphabetically numbered. See also **comment #23**.

21. Figure 20 There is a clear periodicity in figure 20, v – component. Is this due to reconstruction or something else. The periodicity is about 1.8 m ? Also there is some strange signatures of u and v velocity at y/D = 1 and -3 which occurs to be artificial ?

This periodicity is most likely caused by the wind field reconstruction method or interpolation scheme. It will be investigated whether these effects can be filtered out. Also the 'strange signature' is probably caused by invalid measurements. They will be either filtered out or their presence will be discussed.

22. Figure 20 There is distinct different direction on the v-component coming of the rotor comparing turbine 1, 2 and 3. Why ? is there a missed observation ? measurement error due to w-component?

We think that directional differences are mainly caused by the interaction of the multiple wakes. However, this lies beyond the scope of the paper, so it will not be discussed.

23. Figure 21 and 22 Introduce 21 a , 21 b and 22 a and 22 b for clarity.

All subfigures will be alphabetically numbered. See also **comment #20**.

24. p12, section 3.4 I am not wildly convinced the uncertainty analysis is fully representative. The two conditions given on pg. 12 does not include a number of factors. Also there is not consideration of bias errors, which may very well be higher than the uncertainty presented. I appreciate the authors can not give this now, but at least elaborate a bit more on other potential sources and their nature.

It is true that the uncertainty analysis is not representative of all physical effects that possibly have an influence. It is mainly aimed at modeling how a given uncertainty or bias is propagated through the dual-Doppler lidar reconstruction. However, in this way of expressing the error, there is no clear separation between bias and uncertainty. A bias in either the line-of-sight measurement or one of the scanning angles will be propagated in the exact same way. Potential sources for uncertainty and biases will be elaborated on further.

25. Conclusion This: "Because of the lidar measurement principle, between 10-15% of the data is lost due to the moving wind turbine blades in the measurement region" is hardly discussed in the paper, and not what the paper is about. Suggest to strike. It would be prudent to summarize resolution results, frequency and measurement volume over D. Also, comment on future work ?

You are right that the conclusion should not give this new information, without it being mentioned anywhere else. Also the sentence is not clear. Therefore this sentence will be omitted and the data availability will be mentioned somewhere earlier in the paper. Also you stress the importance of concluding on the lidar resolution study, which is valid and will be emphasised in the conclusion in a better way.

Dear anonymous referee,

Thank you very much for your review and your recommendation for publishing this work after a minor revision. We will address all of your comments, which we have numbered 1-13, separately in the following.

1. How did the authors calibrate 3D hot-wire probe? How about accuracy of the calibration? Is there any particular reason for choosing a 3D hot-wire probe even though the lidar measurements were 2D?

    The calibration and accuracy of the hot-wire probes will be stated in the paper more thoroughly. The reason for choosing this device is simply that it was part of the standard setup in the wind tunnel. Also based on the other reviews we received, we will pay more attention to the missing vertical wind speed (w-) component. By using the information of the hot-wire we will be able to address the uncertainty it adds to the reconstructed u- and v-components of the lidar.

2. The authors worry about heating of the hot-wire probe. There have been many studies in literature where LDA and hot-wire or PIV and hot-wire were used in order to measure different flows both in and outside of wind tunnels. Why in this case the heating caused by the laser beam becomes an issue.

    Because we did not know whether or not it could have an influence, we just made sure that the laser beam could not hit the hot-wire itself, as a preventive measure. We believe it is a valid speculation that a laser beam hitting a very sensitive metal wire could interact with it and therefore we focused the beam a small distance away from the hot-wire probe.

3. The authors carried out the measurements of three different types: In the second case, the complete line was covered every 1 s with equally sampled measurements. Here, the characteristics scales of turbulence should be given for quantitative comparison. For example, what is the corresponding integral scale for this 1 s measurements. Is 1 sec statement correct?

    The turbulence scales that can effectively be measured with this setup are larger than the ones corresponding to 1 Hz, because the temporal and spatial resolution are linked. This will be mentioned in the paper.

4. Right before the results the authors give information about the wind velocity profile. Since the work compares the two system, it is of interest to see the velocity and turbulence profiles upstream of the turbines. These profiles should also be compared again the theoretical profiles like the power law instead of giving turbulence intensity at one single location.

    Unfortunately we did not execute measurements of the vertical profile during this measurement campaign. However, a vertical wind profile for both wind speed and turbulence were measured during a previous measurement campaign, under identical conditions. These plots are added to the manuscript.

5. It is not clear why they carried out the measurements at 2500 Hz for hot-wire and 390 Hz for lidar and then compared at 1 Hz. Any particular reasoning for carrying out the measurements this way?

We measured with both devices at their maximum sampling rates, to benefit the most from their turbulence measurements. However, since 2500 Hz and 390 Hz are not compatible, we first averaged the hot-wire measurements to 390 Hz to allow for a fair comparison. But because we know that the lidar probe volume averaging effect filters out small turbulence scales and does not truly resolve turbulence scales up to 390 Hz, also a comparison at a more reasonable 1 Hz was done additionally.

6. It is not clear if the figures 8 and 9 are based on instantaneous readings or the mean quantities, or turbulence. The authors call the figures correlation, but as far as seen in these figures they are individual (or mean) points from one instrument and corresponding reading from the other instrument. How accurate the time lag was introduced intothese computations? Also it is difficult to figure out the motivation for red fits in these figures, 8 and 9. Is there any particular significance? It would also be nice to see how they compute what is presented in figures 8 and 9.

Figures 8 and 9 are regression curves of the wind speed components u and v, showing how well the lidar and the hot-wire probe correlate with each other. We believe that it is standard practice to plot this and fit a regression curve through the scattered points (see the red line). We don't understand what more motivation we should provide for doing so. The plots are based on the instantaneous lidar measurements (390 Hz) and the averaged (from 2500 to 390 Hz) hot-wire measurements. The time lag was computed numerically based on a cross-correlation function, which finds the maximum correlation as a function of time lag. The accuracy of this method is the time step in between the lidar measurements, i.e. 1/390 Hz ≈ 2.6 ms.

7. Figure 10 and 11 show very good agreement between these two signals. Can the authors elaborate effect of down sampling from higher sampling rates on the line plots?

The lidars filter out some small scale turbulence because of the probe length averaging effect. This means that the 390 Hz regression plots are not representative of the capabilities of the lidars. When averaging to 1 Hz, all turbulent scales can be measured as well by the lidar as by the hot-wire probe and the fit becomes better. To investigate this effect further, the plots in Figures 14 and 15 were produced.

8. Discussion regarding the figure 16 needs to be further detailed. For example what is the record length for these spectral computations, and how many blocks of data are used. Even though the Taylors theorem indicates 28 Hz, lidar seems to be rolling off much earlier around at 10 Hz. Any explanation for this? In addition, the authors should write the formulation used for computing spatial averaging when finding 28 Hz. The authors should also write how they computed the spectra.

The spectrum is based on a two minute time series of the 390 Hz data, which is split into ten blocks which are then filtered with a Hann window to smooth the spectrum. This information will be added. The fact that the slope of the lidar spectrum already deviates from the -5/3 Komolgorov rule earlier on is explained with the sentence ,*The drop in the slope of the spectrum does not exactly coincide with the 28 Hz frequency mark, because the intrinsic Lorentzian spatial weighting function of a continuous-wave lidar extends beyond the defined bounds of the probe length, therefore also acting as a filter on lower frequencies.'*. This could be reformulated to increase the clarity.

9. Figure 17 and 18: Here it is interesting to know about how many effective uncorrelated samples in these 1 minute recordings across the wake. Statistical accuracy changes for a fixed record length since the turbulence intensity vary a lot. What do the author mean by binned average? is this average of the open circles?

The red and green lines indeed show the mean and the standard deviation of the measurements marked with grey circles, binned with respect to the y/D-axis. Naturally there is a high uncertainty in the measurements, because the samples might not all be correlated. Therefore the mean profile here is more relevant than the single measurements.

10. The authors note that it is hard to give any hard conclusion on the lidar's ability to measure small scale turbulent fluctuations. Previously the authors showed this when presenting the spectra. According to their approximation the cut-off frequency is about 28 Hz, which is rather low considering the probable length of the cascade, which is hard to find out since the Reynolds number is not stated as far as seen.

We don't have hard numbers for the expected frequency range of the inertial subrange in the case of these wind tunnel measurements. However, the spectrum of the hot-wire probe measurements indicates that it extends roughly from 2 Hz to over 100 Hz, something the lidar measurements are unable to resolve. This difference between the two measurement devices is the most important point here.

You are also indicating that we actually are able to give a quantitative measure of the lidar's ability to measure turbulent fluctuations, namely the cut-off frequency of about 10 Hz (lower than the expected 28 Hz). We will reformulate this accordingly.

11. On page 13 and in line 15, the authors writes about the small scale effect such as wake. What do they mean here? I think it is not possible to capture the small scales using this setup due to the size of measurement volume, and wake itself cannot be considered small scale.

It is true that the wake is not a small scale itself. We meant that normally wakes introduce small scale effects such as a higher turbulence and shear on its boundary. Also we were not able to capture the really small scales in this setup. Therefore the text about this will be rewritten.

12. From the formulation given in the text, it is not obvious that the uncertainty in the y-direction has the most significant contribution. Further explanation is needed for this statement.

The fact that only the gradient $\frac{\delta u}{\delta y}$ was taken into account when assessing the uncertainty introduced by the wake being present, is that the gradient $\frac{\delta u}{\delta x}$ is very small almost everywhere in the wind field. The reason for this is that the wake recovery takes place very gradually, but the boundary of the wake shows very steep gradients along the y-direction. This will be written more clearly in the paper for a better understanding.

13. When the author discuss about the total uncertainty, they mostly relate it to angle difference. Due to the nature of the flow, however, turbulence intensity also plays an important role in any uncertainty computation due to the statistical convergence. Toward the edges of the wake, the mean velocity drops and turbulent fluctuations as well. But the intensity can be very high? What would be the effect of this on their uncertainty calculations. Another question in relation to this one is that the wake develops downstream and velocity deficit gets smaller and smaller, and this leads to stronger demand on resolution. What would be the effect of this on the performance of lidar data, and the uncertainty. One can look at figure 21 and 22 to get an idea, but there the uncertainty is higher along the tip vortex, and wake development does not matter.

It is true that the uncertainty analysis is mostly focusing on the lidar setup, i.e. the difference in the azimuth angle of the two lidars. The emphasis of the uncertainty analysis is the error introduced on the reconstructed wind speed components by the dual-Doppler lidar reconstruction. We do not have reliable measurements of how the turbulence intensity varies over the wind field and in the complex case of the wake, this is surely an important issue. However, this is not regarded here because it is out of the scope of our paper. Therefore a simplified model was established to express the uncertainty added by the wake's deterministic properties.

As stated before, the uncertainty of the dual-Doppler reconstruction is the most important aspect considered here. The wake development does not have a direct effect on the **absolute** value of the uncertainty. If you express it as a percentage of the velocity deficit, the uncertainty will grow, but according to us this is an artificial effect. Therefore we chose to not express the uncertainty in terms of the wake deficit.

Demonstration and uncertainty analysis of synchronised scanning lidar measurements of 2D velocity fields in a boundary-layer wind tunnel

Marijn Floris van Dooren[1], Filippo Campagnolo[2], Mikael Sjöholm[3], Nikolas Angelou[3], Torben Mikkelsen[3], and Martin Kühn[1]

[1]ForWind, University of Oldenburg, Institute of Physics, Oldenburg, Germany
[2]Wind Energy Institute, Technical University of Munich, Garching, Germany
[3]Dept. of Wind Energy, Technical University of Denmark, Roskilde, Denmark

Correspondence to: Marijn Floris van Dooren (marijn.vandooren@uni-oldenburg.de)

Abstract. This paper combines the research methodologies of scaled wind turbine model experiments in wind tunnels with short-range WindScanner lidar measurement technology. The wind tunnel of the Politecnico di Milano was equipped with three wind turbine models and two short-range WindScanner lidars to demonstrate the benefits of synchronised scanning lidars in such experimental surroundings for the first time. The dual-lidar system can provide fully synchronised trajectory scans with sampling time scales ranging from seconds to minutes. First, staring mode measurements were compared to hot-wire probe measurements commonly used in wind tunnels. This yielded goodness of fit coefficients of 0.969 and 0.902 for the 1 Hz averaged u- and v-components of the wind speed, respectively, validating the 2D measurement capability of the lidar scanners. Subsequently, the measurement of wake profiles on a line as well as wake area scans were executed to illustrate the applicability of lidar scanning to the measurement of small scale wind flow effects. An extensive uncertainty analysis was executed to assess the accuracy of the method. The downsides of lidar with respect to the hot-wire probes are the larger measurement probe volume, which compromises the ability to measure turbulence, and the possible loss of a small part of the measurements due to hard target beam reflection. In contrast, the benefits are the high flexibility in conducting both point measurements and area scanning, and the fact that remote sensing techniques do not disturb the flow while measuring. The research campaign revealed a high potential for using short-range synchronised scanning lidars to measure the flow around wind turbines in a wind tunnel, and increased the knowledge about the corresponding uncertainties.

1 Introduction

During the past few years, several research groups have focused attention on wind tunnel experiments with the innovative idea of supporting research not only related to the validation of purely aerodynamic models, but mainly to support numerical activities on control and aero-servo-elasticity (Bottasso et al., 2014) as well as understanding the interaction of wind turbines with turbulent flow (Rockel et al., 2014). In fact, testing of wind turbines in full-scale in the atmospheric boundary-layer imposes several constraints, such as the difficulty in having an accurate knowledge and repeatability of the environmental

1

conditions, higher costs, and especially for public researchers, the difficulty to have access to industrial wind turbines as a research platform. In the same period, academic and industrial researchers have developed new scanning wind lidars able to map full three-dimensional vector wind and turbulence fields in 3D space (Mikkelsen, 2012; Wagner et al., 2015; Simley et al., 2016). Even for complex flows, such as the flow around wind turbines, the lidars can be applied without disturbing the

5　flow itself. The present work reports on the testing activity recently conducted by a joint team of research groups, where two short-range WindScanners have been used in a boundary-layer test section of a wind tunnel for the first time, in order to map the flow of the free chamber as well as to accurately measure the wakes of scaled wind turbine models. Previous research has already been done on wake analysis of full-scale turbines (Iungo and Porté-Agel, 2014; Banta et al., 2015) and in wind tunnels (Lignarolo et al., 2014; Iungo, 2016). Please note that one of the shortcomings of measuring in a wind tunnel with respect to

10　free-field measurements is the poor ability of simulating the variability of atmospheric stability and a representative wind rose.

The objective of the research presented in this paper is to assess the capabilities of continuous-wave short-range lidar to map wind flows and measure turbulence in a wind tunnel. The study has been executed within the larger scope of the CompactWind project, which has the purpose of investigating the effect of different wind farm control concepts and yaw configurations of the individual turbines on the wind farm energy output, the wake structures and wind turbine loads (Campagnolo et al., 2016c).

15　In section 2 about the methodology, the wind tunnel, the model wind turbines, the lidars and the hot-wire probe are described and afterwards the three sequential experiments executed during the measurement campaign are introduced. The results of each of these three experiments are then presented and discussed in section 3, together with an extensive uncertainty analysis. Finally the paper is concluded in section 4.
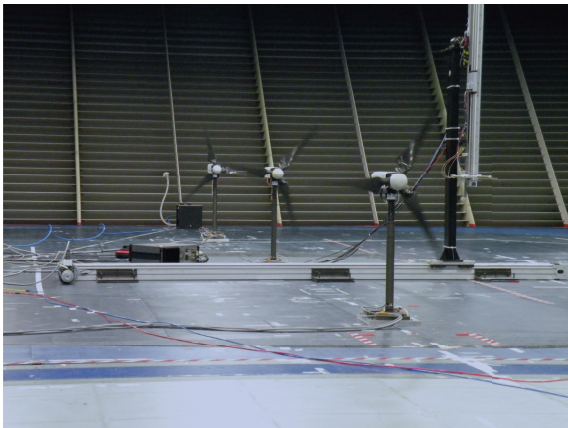

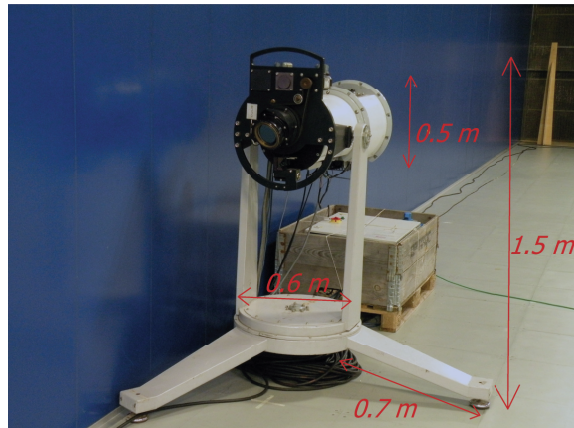**Figure 1.** Model wind turbines in operation in the wind tunnel.

Figure 2. One of the two WindScanner lidars inside the wind tunnel.

20　## 2　Methodology

The experimental setup in the wind tunnel (Bottasso et al., 2014) of the Politecnico di Milano (PoliMi) consisted of three generically scaled wind turbine models (see Fig. 1), named *G1*, specifically designed by the Wind Energy Institute (WEI) at

2

the Technical University of Munich (TUM) for wind farm control research applications (Campagnolo et al., 2016a, b, c), as well as two short-range WindScanners (see Fig. 2) developed by the Department of Wind Energy of the Technical University of Denmark (DTU), joining the common measurement campaign during the last week of January 2016.

2.1 The wind tunnel facility

5 The PoliMi wind tunnel has a closed-return configuration facility arranged in a vertical layout with two test sections. The boundary-layer test section, sketched in Fig. 3, is located at the upper level in the return duct and has a cross-sectional area of 13.84 m by 3.84 m and a length of 36 m, illustrated by the blue outer boundaries. The three wind turbines were mounted on a turn table which allows for rotating the entire turbine array setup, as to create a lateral offset between the wind turbines. When the turn table is in its 'home position', the turbines line up in x-direction with a distance of $4D$ between them. The

10 WindScanners are indicated with red rectangles and their commanded synchronised scan pattern for scanning the wind turbine wakes is plotted in grey. Typical vertical profiles of wind speed and turbulence can be imitated by the use of bricks on the floor that act as roughness and turbulence generators, i.e. spires, placed at the chamber inlet at the left boundary. For more information about the wind tunnel, please refer to Zasso et al. (2005).
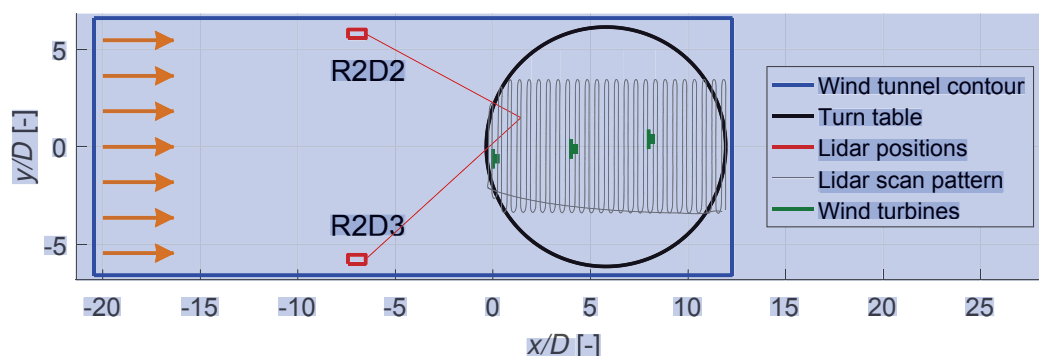
Figure 3. Configuration of the wind tunnel of the Politecnico di Milano with the two scanning lidars and the three model wind turbines installed on the turn table. The axes are normalised with respect to the wind turbine diameter of $D = 1.1$ m.

The inflow conditions in the wind tunnel were kept constant throughout the measurement campaign. The free-stream wind
15 speed and the turbulence intensity, both at hub height, were $u_\infty = 5.67$ m s^{-1} and $TI = 5.5\%$, respectively. Figures 4 and 5 illustrate vertical profiles of the inflow wind speed and turbulence intensity, respectively, measured during a highly similar measurement campaign. The vertical wind profile corresponds to a power law profile with shear exponent $\alpha = 0.09$.
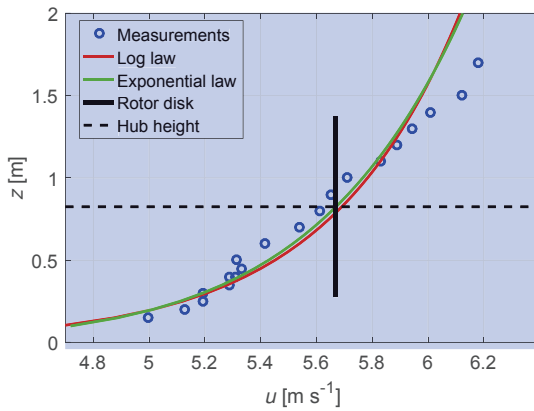
3

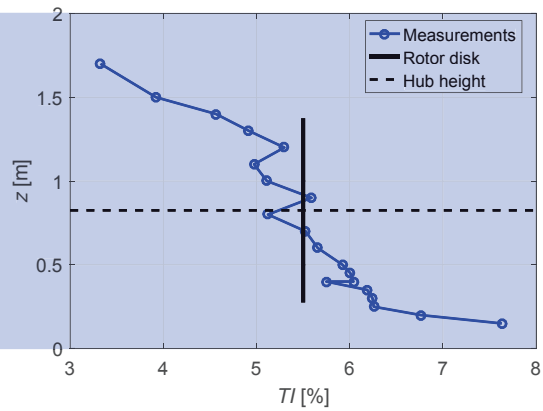**Figure 4.** Vertical profile of the inflow velocity.

Figure 5. Vertical profile of the inflow turbulence intensity.

2.2 The G1 wind turbine models

The three scaled *G1* wind turbine models have a rotor diameter D of 1.1 m, a hub height of 0.825 m and a rated rotor speed equal to 850 rpm. They were designed to provide a realistic energy conversion process, which means reasonable aerodynamic
5 loads and damping with respect to full-scale wind turbines, as well as wakes with a realistic geometry, velocity deficit and turbulence intensity. Moreover, systems have been integrated to enable individual blade pitch, torque and yaw control, while a sufficient onboard sensor equipment of the machine, providing measurements of rotor azimuth angle, main shaft loads, rotor speed and tower base loads, enables the testing of both wind turbine and wind farm control strategies.

Each *G1* model is equipped with three blades whose pitch angles can be varied by means of brushed motors housed in the
10 hollow roots of the blades and commanded by dedicated electronic control boards housed in the hub spinner. Electrical signals from and to the pitch control boards are transmitted by a through-bore 12-channels slip ring located within the rectangular carrying box holding the main shaft. A torque sensor allows for the measurement of the torque provided by a brushless motor located in the rear part of the nacelle, which is operated as a generator by using a servo-controller. An optical encoder, located between the slip ring and the rear shaft bearing, allows for the measurement of the rotor azimuth angle. The tower is softened
15 at its base by machining four small bridges, on which strain gauges are glued so as to measure fore-aft and side-side bending moments. Aerodynamic covers of the nacelle and hub ensure a satisfactory quality of the flow in the central rotor area.

Each *G1* model is controlled by an *M1 Bachmann* hardware real-time module. Similarly to what is done on real wind turbines, collective or individual pitch-torque control laws are implemented on and real-time executed by the control hardware. Sensor readings are used online to properly compute the desired pitch and torque demands, which are in turn sent to the actuator
20 control boards via analog or digital communication.

4

2.3 The short-range WindScanner lidars

The two short-range WindScanners R2D2 and R2D3, installed near the section walls upwind of the turbine models (see Fig. 3), are continuous-wave, coherent lidars that can provide Doppler spectrum averaged wind speeds at rates up to 390 Hz. The measurement range is defined by the optical configuration of the device, which enables motor controlled focus distance between

5 about 10 m and 150 m. The longitudinal line-of-sight sampling volumes can become very small at short ranges, e.g. about 13 cm probe length at a 10 m focus distance, thus the WindScanners were placed as close as possible to the measurement area of interest, within the reachable focus distances. The laser beam can be freely steered within a cone with a full opening angle of 120° by the use of two prisms. The two prism motors and focus motor that each lidar comprises are synchronously operated by a common central multi-axis motion controller that steers all the six motors such that the two focused laser beams can

10 synchronously follow a common scanning trajectory. The relation between the motor positions and the measurement location relative to each WindScanner was pre-calibrated at DTU leaving only the location and orientation of the WindScanners relative to the measurement scene to be determined in the deployment situation. The scan heads of R2D2 and R2D3 were placed at $(x = -7.17 \text{ m}, y = 6.36 \text{ m}, z = 1.31 \text{ m})$ and $(x = -7.18 \text{ m}, y = -6.34 \text{ m}, z = 1.30 \text{ m})$, respectively, and the instruments were tilted by 90.148° and 90.123°, respectively. The symmetry axes of the scan heads were roughly aligned with the x-axis, i.e.

15 with azimuth directions relative the x-axis of -0.111° and 0.021°, respectively. The detailed positions where obtained by a Leica total station and the orientation was obtained by the similarly determined detailed positions of small rotating balls placed close to the wind tunnel outlet and providing distinct hard target Doppler returns. An additional verification of the measurement locations close to the turbines was done by imaging the laser beam on a reflective plane by an infrared-sensitive camera.

Each lidar measures a projected line-of-sight component of the three-dimensional wind velocity vector. From two temporally

20 and spatially synchronised line-of-sight measurements v_{LOS}, the u- and v-components of the wind speed, defined along and lateral to the main wind direction respectively, can be calculated by solving the linear equation system in Eq. (1):

$$\begin{bmatrix} \cos(\chi_1)\cos(\delta_1) & \sin(\chi_1)\cos(\delta_1) \\ \cos(\chi_2)\cos(\delta_2) & \sin(\chi_2)\cos(\delta_2) \end{bmatrix} \begin{bmatrix} u \\ v \end{bmatrix} = \begin{bmatrix} v_{LOS_1} \\ v_{LOS_2} \end{bmatrix} \tag{1}$$

The horizontal and vertical scanning angles of a lidar system are the azimuth χ and elevation δ angles, respectively. The vertical wind component w is omitted, since a third lidar would be needed to evaluate this additional component. Because the

25 lidar scan heads are located slightly higher than the turbine hub height, small negative elevation angles of up to $\delta < 3°$ had to be used. This could create a bias of $\sin(3°)w$ on the measured v_{LOS}.

As mentioned before, the lidars acquire each measurement based on the aerosols present in a certain probe volume, which is illustrated qualitatively in Fig. 6. The value of the probe length is commonly defined as twice the Half Width Half Maximum Γ, which is the distance at either side of the focus point at which the backscatter signal power is reduced to half of its maximum

30 power. The power spectrum of the backscattered signal can be expressed with a Lorentzian probability distribution along the beam line-of-sight direction, multiplied by the line-of-sight wind speed component at the corresponding coordinates. The probe length increases quadratically with the focus distance, which is expressed in Eq. (2) and plotted in Fig. 7. In Eq. (2), Γ is the

Half Width Half Maximum, λ is the lidar laser wavelength (1.565 μm, infrafred), f is the focus distance and a is the laser beam width at the aperture (28 mm). Throughout the measurement campaign focus distances between 10 m and 20 m were used, yielding probe lenghts of 13 cm and 50 cm, respectively. These marks are indicated in Fig. 7.
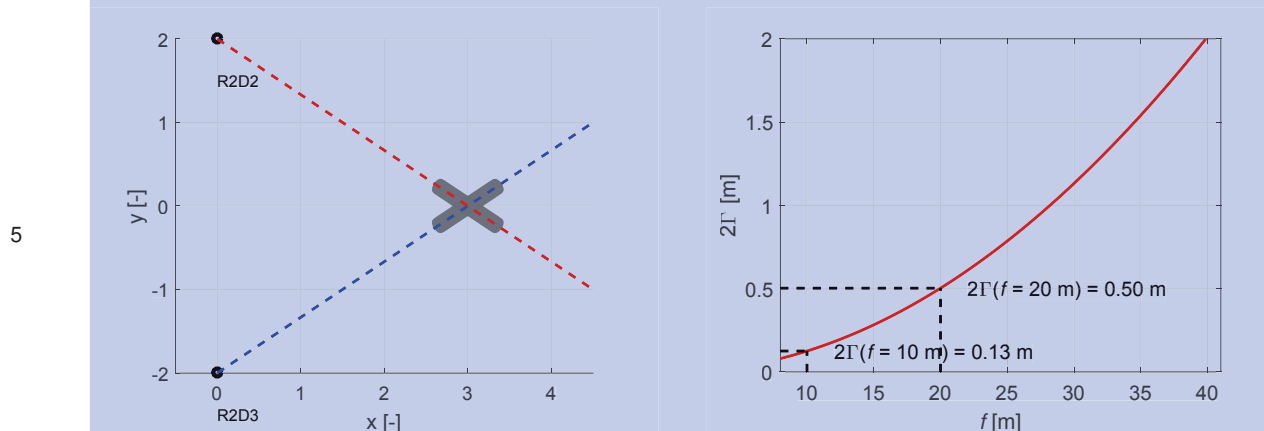
$$\Gamma = \frac{\lambda f^2}{\pi a^2} \tag{2}$$

5

Figure 6. Sketch of the probe volumes of both lidars (not to scale). **Figure 7.** Relationship between focus distance and the probe length.

2.4 The hot-wire probe

A tri-axial Dantec 55R91 hot-wire probe (see Fig. 8) was mounted on an automatic traversing system (see Fig. 9) and provided 2500 Hz measurements of the three-dimensional wind speed vector in the wind tunnel. The three wires of the hot-wire probe form an orthogonal system with respect to each other and are also positioned orthogonally to the prongs of the probe for

10   increased accuracy. The effective sensor length of each of the wires is 1.25 mm. The calibration of the hot-wire probes was performed in the 150-by-200 mm^2 closed test section within the PoliMi wind tunnel facility, with a contraction ratio of 25. The calibration procedure consists of the following three steps:

1. The probe in positioned in the wind tunnel, whose flow velocity is calculated from the dynamic pressure, measured with a pressure transducer of the type *Druck LPM9481*, and the density, in turn calculated using accurate measurements of

15   the relative humidity and absolute pressure.

2. The alignment of the probe support to the wind tunnel flow is assured by means of an inclinometer of the type *Spectron L-212T*.

3. The Jørgensen (2002) Law is applied, which follows the hypothesis of decoupled directional response and velocity magnitude response of the probe.
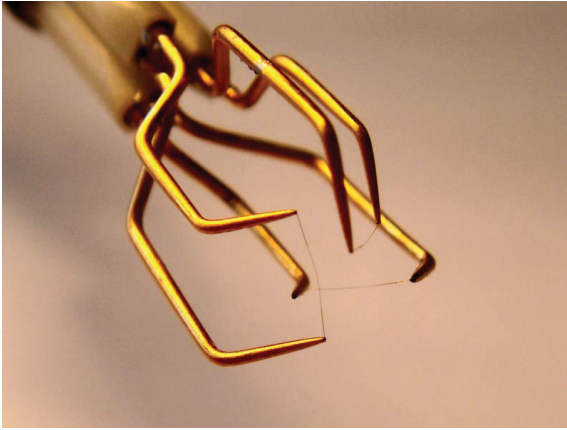
6

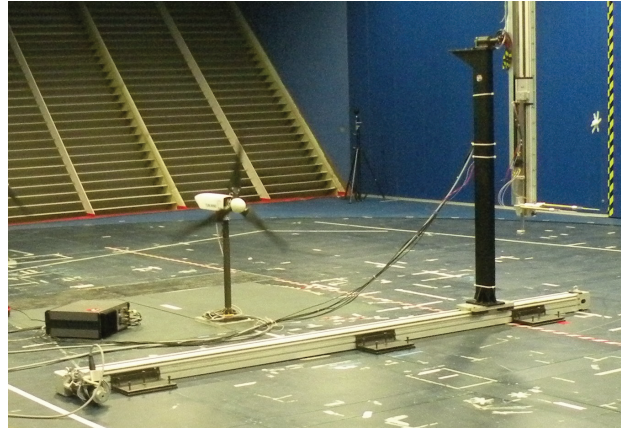**Figure 8.** The tri-axial Dantec 55R91 hot-wire probe.

Figure 9. The traversing system for the hot-wire probes.

2.5 Measurement examples

The measurement campaign covered several scenarios. In this paper, only relevant examples from the three main types of measurements are presented to illustrate the capabilities:

5   1. *Comparison between lidar and hot-wire probe measurements*: The lidar beams were focused as closely to the hot-wire as practically possible, i.e. without influencing the hot-wire probe due to heating by the laser beams on the one hand, or blocking the view of the lidars with the hot-wire probe and the traversing system on the other. The focus offset was chosen to be 2 cm. A series of different points in the wind tunnel were measured by both anemometers for a duration of 2 minutes each. In this case, the data of a single point at $x = 2.23$ m, $y = 0.88$ m, $z = 0.83$ m is considered for analysis.

10   The wind turbines were idling at approximately 80 rpm, which is assumed to have a negligible effect on the flow.

2. *Measurement of wake profiles along a horizontal line*: The lidars performed measurements back and forth along cross-wind lines at several distances downstream of the first wind turbine at hub height and spanning $\pm 3.5D$ around the wake centre. The complete line was covered every 1 s with equally sampled measurements. In the case presented, a wake profile at a $3D$ downstream distance of the first wind turbine is analysed. This turbine was operating with an average

15   rotor speed of 805 rpm, average pitch angle of 0.4°, C_p of 0.38, C_T of 0.83 and had a yaw offset of 20°.

3. *Measurement of horizontal wake area scans*: The full area containing the three wakes of the model turbines was mapped by the lidars by iterating through the scanning pattern indicated previously in Fig. 3. The scans cover an area of 7 m by 13 m every 18.5 s. Multiple scans were averaged to resolve the mean wake features. None of the wind turbines had a yaw offset. The first turbine had an average rotor speed of 830 rpm, average pitch angle of 0.55°, C_p of 0.42 and C_T of 0.88.

20   The second and third turbine had average rotor speeds of 710 and 736 rpm, respectively. No C_p and C_T were recorded.

7

3 Results

3.1 Comparison between lidar and hot-wire probe measurements

The first step of the lidar campaign in the wind tunnel was to establish a quantitative measure of the accuracy of the lidars with respect to the commonly applied devices in such an environment, i.e. hot-wire anemometers. Here, the established hot-wire probe served as a validation for the lidar measurements. In order to compare the devices directly with each other, the hot-wire probe data recorded at 2500 Hz has been averaged to match the lidar measurement frequency of 390 Hz. Subsequently, the data of both devices was averaged to 1 Hz and compared again.

Table 1. Comparison of the statistics of the 390 Hz and 1 Hz wind speed components measured at a point over a 2-minute time frame by the hot-wire probe and the lidars.

	Hot-wire 390 Hz			Lidar 390 Hz		Hot-wire 1 Hz			Lidar 1 Hz	
	u	v	w	u	v	u	v	w	u	v
μ [m s^{-1}]	5.67	-0.04	0.08	5.65	-0.03					
σ [m s^{-1}]	0.31	0.28	0.26	0.28	0.27	0.15	0.07	0.08	0.16	0.07
γ_1 [-]	-0.05	-0.16	-0.03	-0.21	0.67	-0.09	-0.24	0.02	-0.13	-0.29
γ_2 [-]	3.17	3.03	3.03	4.55	15.13	3.14	3.02	2.69	3.03	3.20

In Table 1 the mean (μ), standard deviation (σ), skewness (γ_1) and kurtosis (γ_2) of the u-, v-, and w-components from a single 2-minute point measurement time series of both systems can be seen, for the 390 Hz time series and the 1 Hz averaged time series. The u-, v- and w-components are expressed in the x-, y- and z-direction of the lidar reference frame, respectively, which is indicated in the wind tunnel configuration sketch (see Fig. 3). The hot-wire probe measurements originally obtained in a different coordinate system were transformed into the lidar frame of reference. Time synchronisation between the devices was taken care of by a cross-correlation optimisation procedure.

The u-, v- and w-components of the hot-wire are directly measured and the u- and v-components of the lidars are derived from the line-of-sight measurements by applying Eq. (1). It cannot be confirmed with certainty whether the nonzero v- and w-components are a flow feature or stem from an instrument misalignment. The w-component cannot be evaluated from the lidar measurements in this case and is therefore neglected. Doing this may cause a slight bias on the u- and v-components measured by the lidars, since on average there is a vertical wind speed of 0.08 m s^{-1}. It was mentioned before that the measured v_{LOS} will be affected by a bias of $\sin(3°)w$, which gets propagated through Eq. 1.
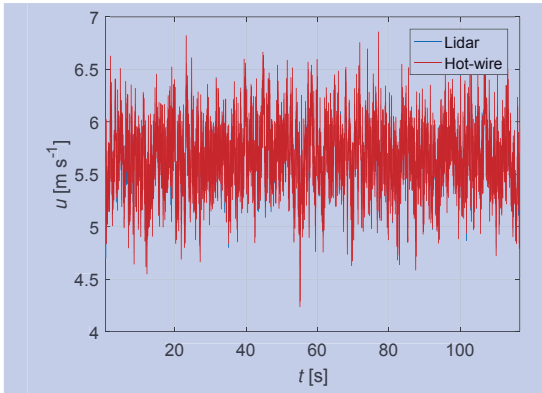
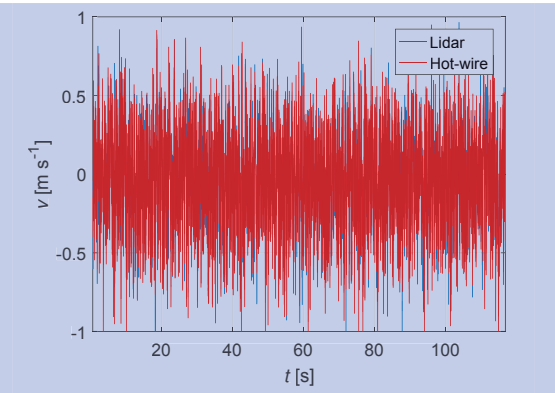**Figure 10.** Visual comparison of the 390 Hz u-component.

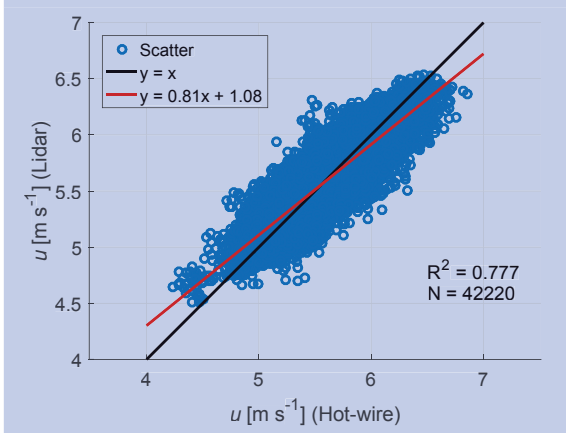**Figure 11.** Visual comparison of the 390 Hz v-component.

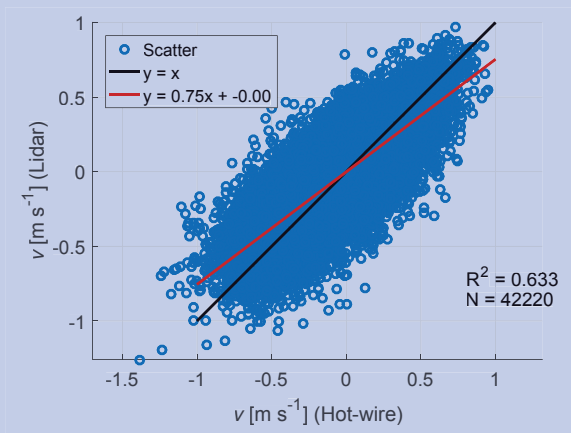**Figure 12.** Correlation of the 390 Hz u-component.

Figure 13. Correlation of the 390 Hz v-component.

Time series of the 390 Hz u- and v-components of both the lidar and the hot-wire probe can be seen in Figs. 10 and 11, respectively. The signals are hard to distinguish from each other, because of the good correlation. Correlation plots of both the u- and v-components are shown in Figs. 12 and 13, respectively. Although the regression line does not perfectly resemble $x = y$ and some scattering is visible, the measurements yielded very reasonable - especially for the considered sampling rate - goodness of fit coefficients of $R^2 = 0.777$ for the u-component and $R^2 = 0.633$ for the v-component. A possible reason for the remaining scatter in the plot is the difference in the probe volumes of the anemometers. They are not measuring in the exact same point or volume, so different fluctuations are seen by the different devices. The biases in the slope and the offset could be caused by neglecting the contribution of the w-component on the measured v_{LOS}. Also there might be a small bias in the transformation between the different coordinate systems of the lidars and the hot-wire probe, causing a cross-contamination in the calculation of both wind speed components u and v.
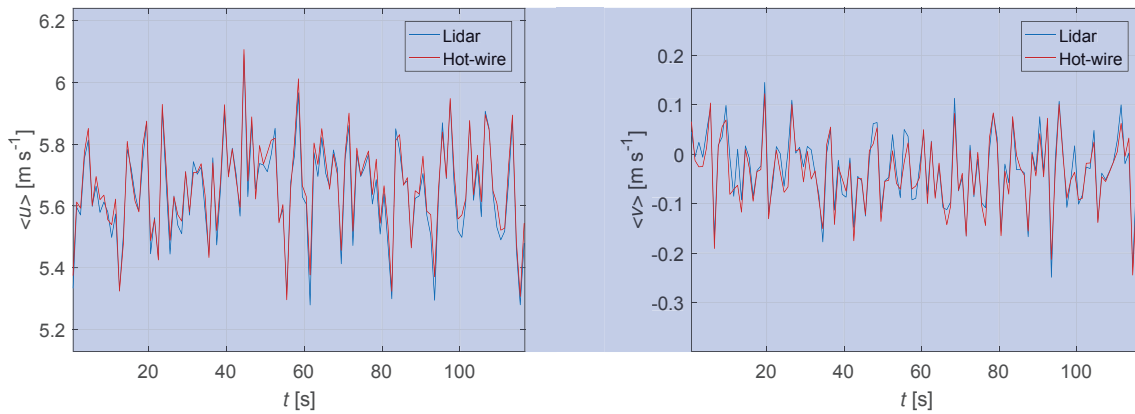
Figure 14. Visual comparison of the 1 Hz averaged u-component.   **Figure 15.** Visual comparison of the 1 Hz averaged v-component.

The time series were subsequently further averaged to 1 Hz data. Figures 14 and 15 display the u- and v-components of both anemometers, respectively. On this time scale, it can be concluded visually that the measurements correlate very well. The 1 Hz averaged u- and v-components in Figs. 14 and 15 were correlated with each other, as shown by Figs. 16 and 17.
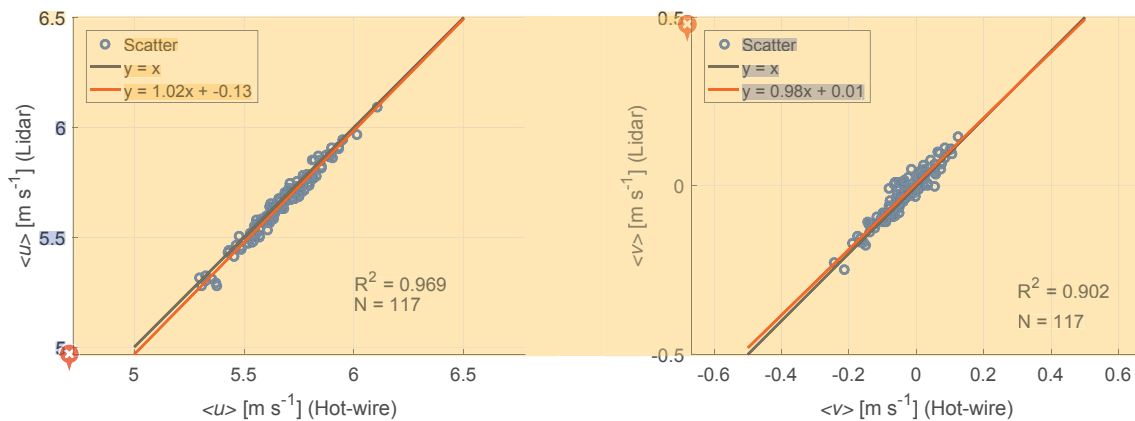

Figure 16. Correlation of the 1 Hz averaged u-component.   **Figure 17.** Correlation of the 1 Hz averaged v-component.

The mentioned effects that caused the scatter in the correlated 390 Hz data of Figs. 12 and 13 do not play a large role anymore after the data has been averaged to 1 Hz time series, since small scale fluctuations are averaged out. Correlating the 1 Hz averaged data now provided the goodness of fit coefficients of $R^2 = 0.969$ for the u-component and $R^2 = 0.902$ for the v-component, which can be regarded as a definite validation of the lidar measurements in the wind tunnel at 1 Hz. The fact that both components at 1 Hz follow the same trend, is a confirmation of the good synchronisation of the WindScanners.
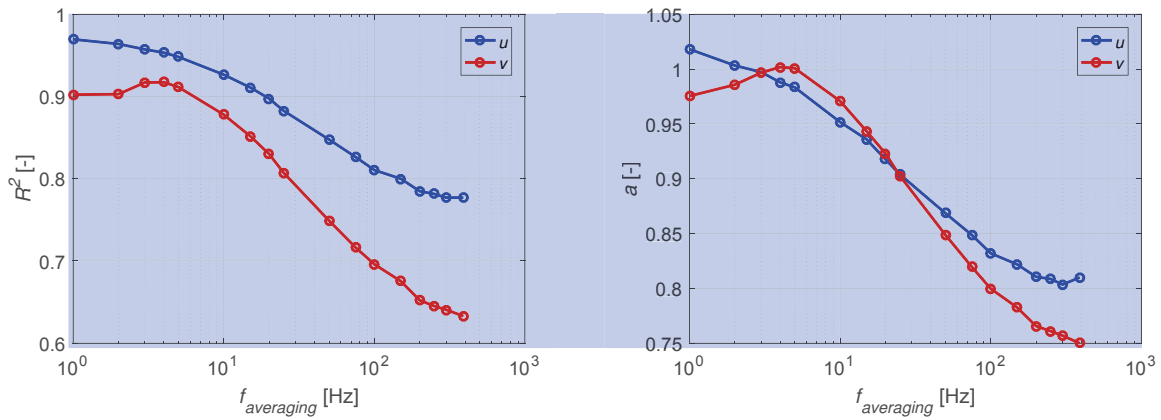
10

Figure 18. Goodness of fit parameter R^2 of the linear fit between the averaged u- and v-components of the lidar and the hot-wire as a function of averaging frequency.

Figure 19. Slope a of the linear fit between the averaged u- and v-components of the lidar and the hot-wire as a function of averaging frequency.

Figures 18 and 19 show the influence of the averaging frequency on the goodness of fit R^2 and the regression line slope a of the linear fit, respectively. As expected, a better fit is yielded for lower averaging frequencies. In case of wake measurements, it is important that the lidars are able to resolve the fluctuation scales induced by the wind turbines. Since the rated rotor speed is equal to 850 rpm, which is approximately 14 Hz, also the time series with this averaging rate were compared. The goodness of fit coefficients were $R^2 = 0.916$ for the u-component and $R^2 = 0.860$ for the v-component in this case.

To analyse the capability of measuring turbulence with lidars (Sathe and Mann, 2013), the spectra of the u-component of both the lidar and the hot-wire are plotted in Fig. 20. The spectra are based on the full two minute time series of the 390 Hz data, which is split into ten blocks, filtered with a Hann window for smoothing, and then averaged. Since the sampling frequencies of the hot-wire probe and the lidars are 2500 Hz and 390 Hz, respectively, the boundary of the plot was chosen to be the Nyquist frequency based on the lidar, which equals 195 Hz. The lidar measurements are based on the backscatter of aerosols in a small measurement volume with a length of approximately 13 cm and therefore turbulent structures with a size smaller than this measurement probe volume are partly filtered out. By applying Taylor's Theorem (Taylor, 1938) one can calculate that the lidars can resolve temporal turbulence scales up to $\frac{1}{2} \cdot 5.67$ m s^{-1}/0.13 m = 22 Hz in this case. This line is marked in Fig. 20. It can be seen that the lidar indeed shows less power in the spectrum than the hot-wire for the upper frequency range. The drop in the slope of the spectrum does not exactly coincide with the 22 Hz frequency mark, because the intrinsic Lorentzian spatial weighting function of a continuous-wave lidar extends beyond the defined bounds of the probe length, therefore also acting as a filter on lower frequencies. The effect of spatial weighting is explained in detail by Sjöholm et al. (2009). Also combining measurements from two lidars that each have a different probe volume causes an even larger effect of averaging out small turbulence scales over a more complex x-shaped volume (see Fig. 6).
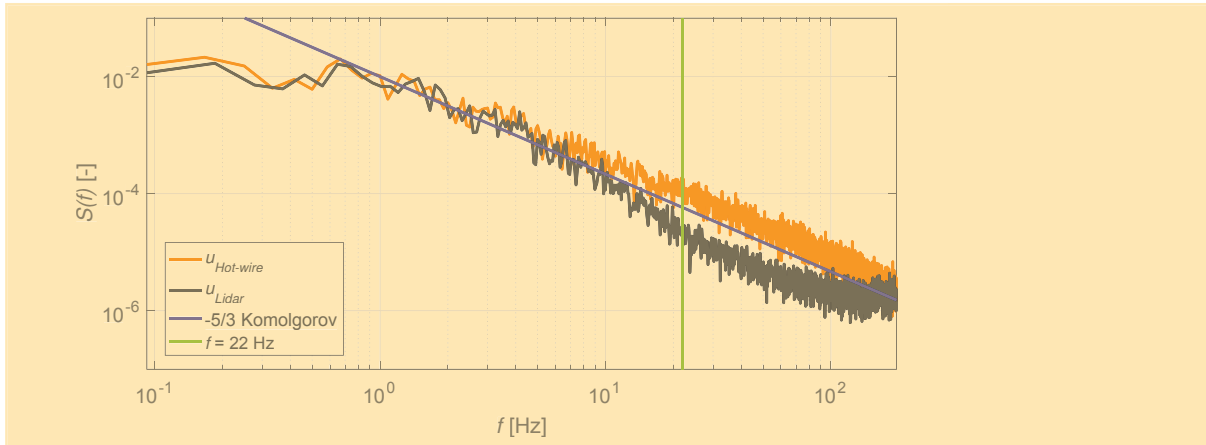
11

Figure 20. Turbulence spectrum of the u-component.

3.2 Measurement of wake profiles along a horizontal line

In Figs. 21 and 22, the respective u- and v-components of the wind speed evaluated from the line-of-sight measurements of both lidars of the transverse wake profile at hub height at a distance of $3D$ downstream of the first turbine can be seen. Both components are normalised with respect to the free-stream velocity $u_\infty = 5.67$ m s^{-1}. The data availability was 87.9%, due to the hard target signal return of the wind turbine blades. All single measurements recorded with 390 Hz over a 1-minute period are plotted, as well as a bin averaged line with its standard deviation ($\pm 1\sigma$) bounds. The scatter of the measurements is reasonable and a smooth wake profile is produced. It is interesting to note that the v-component is almost zero on average, but it has a highly turbulent behaviour at the wake boundaries. This is probably caused by the high velocity gradients and the increased turbulence intensity at the boundaries of the wake.
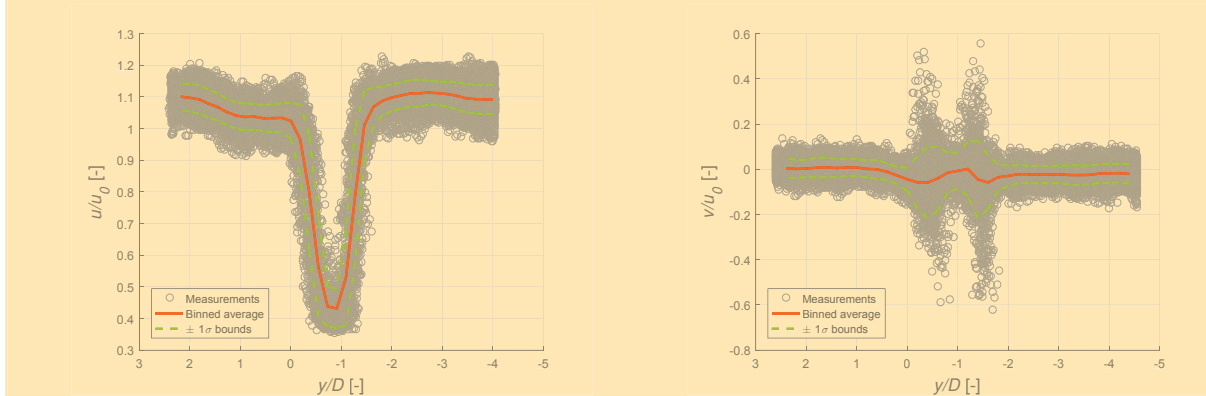
Figure 21. Wake profile expressed in the evaluated u-component, at $3D$ behind the first turbine with a 20° yaw angle.

Figure 22. Wake profile expressed in the evaluated v-component, at $3D$ behind the first turbine with a 20° yaw angle.

12

3.3 Measurement of horizontal wake area scans

The WindScanners can follow synchronised scan patterns that cover any desired plane or volume in space. The scanning pattern sketched in Fig. 3 was used to map a horizontal plane at hub height containing the wake of all three wind turbines. Note that at the far end of the scan, the lidar units are measuring at a focus distance of about 20 m, which results in a probe length of about 50 cm locally. In Fig. 23 the normalised line-of-sight component measured by R2D3 is plotted, as the result of one scan iteration (Fig. 23a) and as an average of 30 scan iterations (Fig. 23b). This amount of iterations corresponds approximately to a 10-minute period. Although some blocking of the data is expected from the moving wind turbine blades, still the measurement availability after filtering of 89.4% is satisfying. The normalised u- and v-components, calculated through Eq. (1), are plotted in Figs. 24a and 24b, respectively. It illustrates that the lidars are capable of determining the two-dimensional flow across a horizontal wind turbine wake cross-section. The plot of the u-components shows a smooth and overlapping triple wake, enabled by the low turbulence in the wind tunnel. The non-zero local v-components are indicating the initial flow expansion in the induction zone of each of the turbines. These effects are well visible in the upper part of the plot, whereas in the lower part of the wake these effects are averaged out due to the larger turbulence in the region where the wakes from the three turbines partly overlap. Some artefacts can be seen in the background of Fig. 24b, probably caused by interpolation.
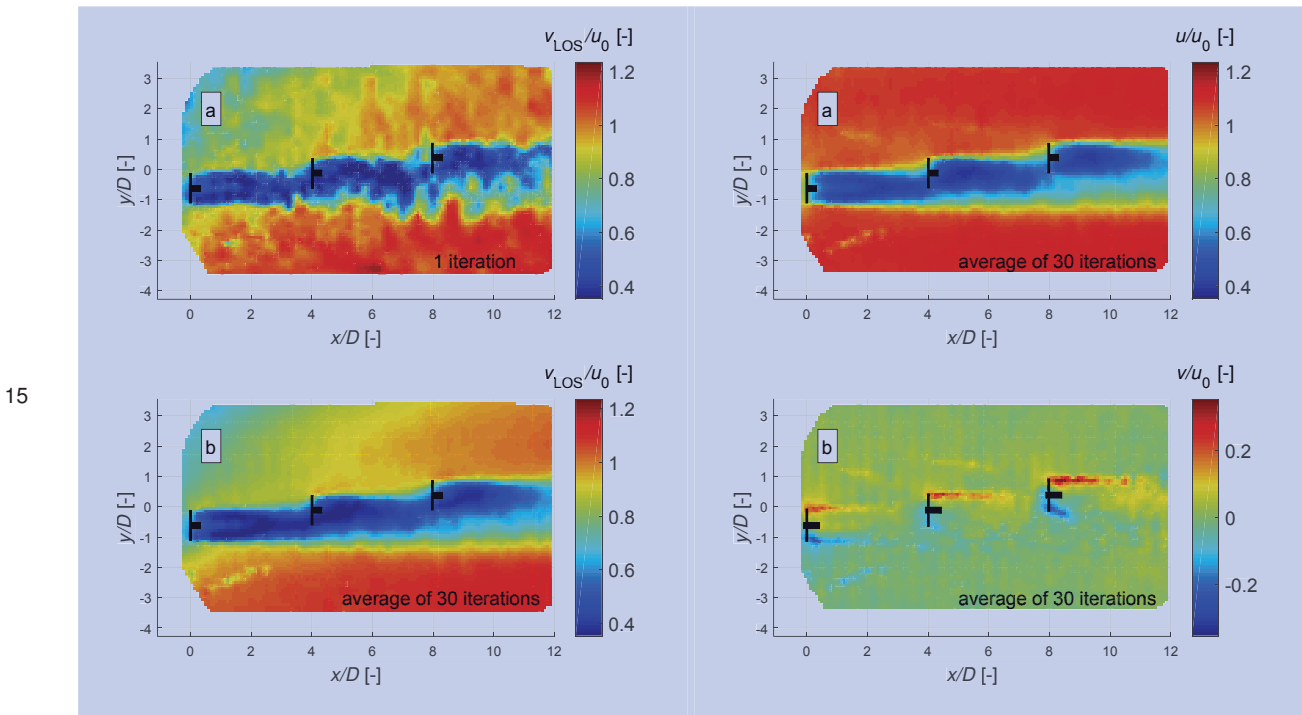

Figure 23. Wake wind field expressed in the line-of-sight component of R2D3, for **a**: 1 iteration, **b**: average of 30 iterations.

Figure 24. Wake wind field expressed in the evaluated u- and v-components; **a**: u, **b**: v.

13

Note that it is hard to give any hard conclusions on the lidars' ability to measure small-scale turbulent fluctuations for this case, since the temporal resolution of the scans is not sufficient to track them. The wind field 'refreshing time' is in the order of a few seconds, whereas a single scan took 18.5 s to complete. This is a direct consequence of the small scale of the experiment and the trade-off that was made between spatial and temporal resolution.

3.4 Uncertainty analysis

It is of particular interest how the dual-Doppler reconstruction affects the uncertainty of the estimated u- and v-components, according to a standard uncertainty propagation method (JCGM, 2008). Similar analyses have already been carried out by Stawiarski et al. (2013) and van Dooren et al. (2016). The method described here considers both the lidar measurement uncertainty itself, as well as the artificially added uncertainty of the dual-Doppler reconstruction. The inputs are:

1. The uncertainty of the measured line-of-sight wind speed $e_{v_{LOS}}$, conservatively assumed to be 1% (Pedersen et al., 2012) of the free-stream velocity (= 0.0567 m s^{-1}), plus the worst-case bias of $\sin(3°)w$ (= 0.0523 m s^{-1}) on the measured v_{LOS} that could be caused by neglecting a maximum w-component of 1 m s^{-1} (as measured by the hot-wire probe). This is a conservative estimate, which makes sure all possible error sources are included.

2. The pointing error for both the elevation and azimuth angles, e_δ and e_χ respectively, assumed to be 0.5 mrad ($\approx 0.03°$).

By solving the linear system in Eq. (1), one can express the quantities u and v individually:

$$u = \frac{\sin(\chi_2)\cos(\delta_2)v_{LOS_1} - \sin(\chi_1)\cos(\delta_1)v_{LOS_2}}{\cos(\delta_1)\cos(\delta_2)\sin(\chi_2 - \chi_1)} \tag{3}$$

$$v = \frac{\cos(\chi_1)\cos(\delta_1)v_{LOS_2} - \cos(\chi_2)\cos(\delta_2)v_{LOS_1}}{\cos(\delta_1)\cos(\delta_2)\sin(\chi_2 - \chi_1)} \tag{4}$$

The numerical errors e_u and e_v of the respective velocity components u and v are then expressed as follows:

$$e_u = \sqrt{\left(\frac{\partial u}{\partial v_{LOS_1}}e_{v_{LOS_1}}\right)^2 + \left(\frac{\partial u}{\partial v_{LOS_2}}e_{v_{LOS_2}}\right)^2 + \left(\frac{\partial u}{\partial \chi_1}e_{\chi_1}\right)^2 + \left(\frac{\partial u}{\partial \chi_2}e_{\chi_2}\right)^2 + \left(\frac{\partial u}{\partial \delta_1}e_{\delta_1}\right)^2 + \left(\frac{\partial u}{\partial \delta_2}e_{\delta_2}\right)^2} \tag{5}$$

$$e_v = \sqrt{\left(\frac{\partial v}{\partial v_{LOS_1}}e_{v_{LOS_1}}\right)^2 + \left(\frac{\partial v}{\partial v_{LOS_2}}e_{v_{LOS_2}}\right)^2 + \left(\frac{\partial v}{\partial \chi_1}e_{\chi_1}\right)^2 + \left(\frac{\partial v}{\partial \chi_2}e_{\chi_2}\right)^2 + \left(\frac{\partial v}{\partial \delta_1}e_{\delta_1}\right)^2 + \left(\frac{\partial v}{\partial \delta_2}e_{\delta_2}\right)^2} \tag{6}$$

The first two terms of the square root, i.e. containing the partial derivatives with respect to the line-of-sight speed, formed the largest contribution to both e_u and e_v. The derivatives with respect to the scanning angles had less influence for the current measurement setup in combination with the assumed numerical values of the uncertainties.

To include the uncertainty introduced by measuring in the wind turbine wake region, which is characterised by large spatial gradients, the 10-minute averaged wind fields are used to estimate these gradients and execute a precision study on the effect of

a small pointing error on the actual measurement. Especially at the far end of the measurement domain, a small angular offset of 0.03° could cause a dislocation of the measurement point in the y-direction of 1 cm. When measuring a small scale effect in a wake, this displacement could affect the uncertainty significantly. In the following, we only consider the uncertainty in the y-direction, assuming this has the most significant contribution. Namely, the gradients in this direction are much steeper than

5 in the x-direction, with an exception for the near vicinity of the rotor plane.

The uncertainty e_y can be expressed in the azimuth angle pointing accuracy as follows:

$$e_y = \left(\sin\left(\chi + \frac{1}{2} e_\chi \right) - \sin\left(\chi - \frac{1}{2} e_\chi \right) \right) f \tag{7}$$

With this information, we are able to include an error on the u-component of the velocity according to the gradients in y-direction by means of the following uncertainty estimate:

10 $$e_{u_{wake}} = \frac{\partial u}{\partial y} e_y \tag{8}$$

The partial derivative $\frac{\partial u}{\partial y}$ is calculated numerically with a first order central finite difference coefficient based on the 10-minute averaged measurement itself (see Fig. 24a).
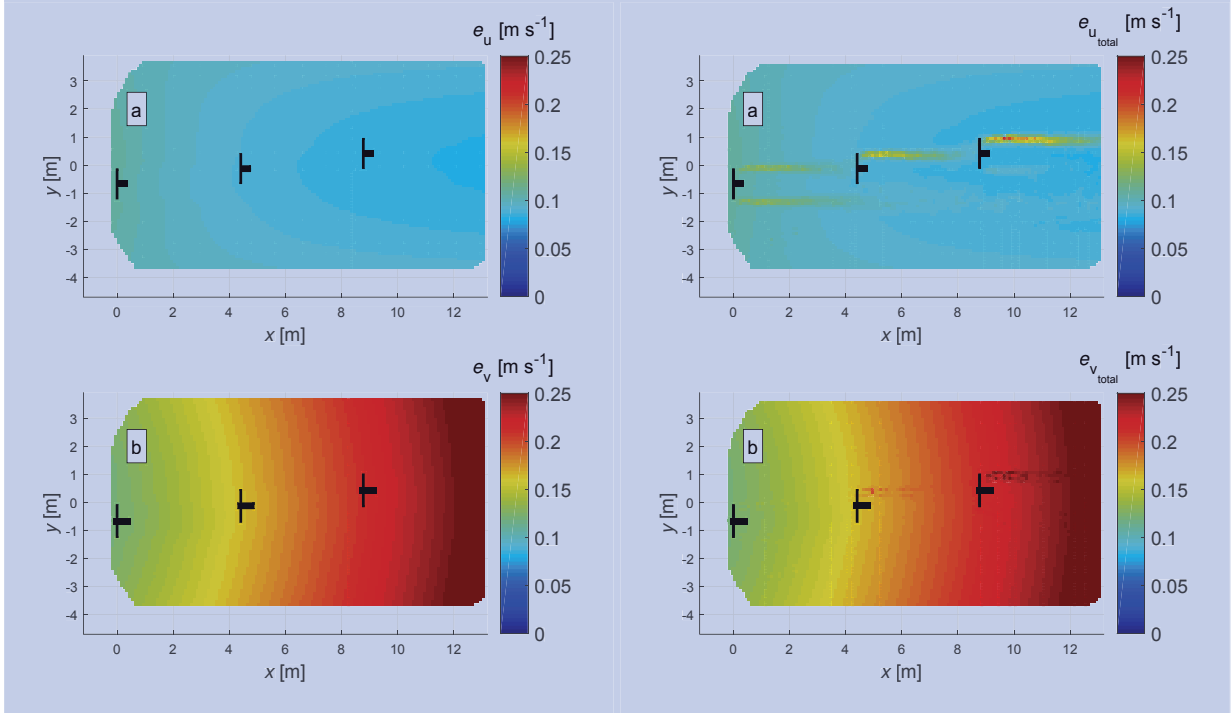

Figure 25. Dual-Doppler uncertainty on the evaluated u- and v-components; **a**: u, **b**: v.

Figure 26. Dual-Doppler uncertainty on the evaluated u- and v-components including wake gradient error; **a**: u, **b**: v.

15

Finally, the total uncertainty including the wake effect can be calculated as such:

$$e_{u_{total}} = \sqrt{e_u^2 + e_{u_{wake}}^2} \qquad (9)$$

In Figs. 25a and 25b the 10-minute averaged uncertainty plots of both the evaluated u- and v-components, e_u and e_v respectively, are presented. It can be seen that the error e_v is larger than e_u overall. In the plot of e_u it can be seen that the

5 error decreases slightly while moving from left to right. This is caused by the better alignment of the lidar beams with the x-direction. More interesting to analyse is the error on the v-component. It shows a significant increase towards the right of the measurement domain. This is related to the difference in azimuth angles between the two lidars, i.e. the lidar beams become more aligned with each other and thus have less potential to accurately resolve two orthogonal wind speed components. When the difference between the azimuth angles $|\Delta\chi| = |\chi_1 - \chi_2|$ tends towards $180°$, the u-component cannot be resolved anymore

10 and when $|\Delta\chi|$ tends towards $0°$, this applies to the v-component. To the far left of our measurement domain, $|\Delta\chi| \approx 90°$, which is the ideal case for dual-Doppler wind field reconstruction. To the far right of the plot, this angle difference decreases to $|\Delta\chi| \approx 30°$.

In Fig. 26 the respective total uncertainties $e_{u_{total}}$ are plotted, which include an error component related to the wake boundary gradients. As expected, an increased uncertainty around the boundaries is calculated, which gets larger with increasing distance

15 from the lidars. Particularly interesting is that on the lower part of the plots, the overlapping wakes from the three wind turbines smooth out the gradients, causing the error to be smaller than at the upper and steeper wake boundaries.
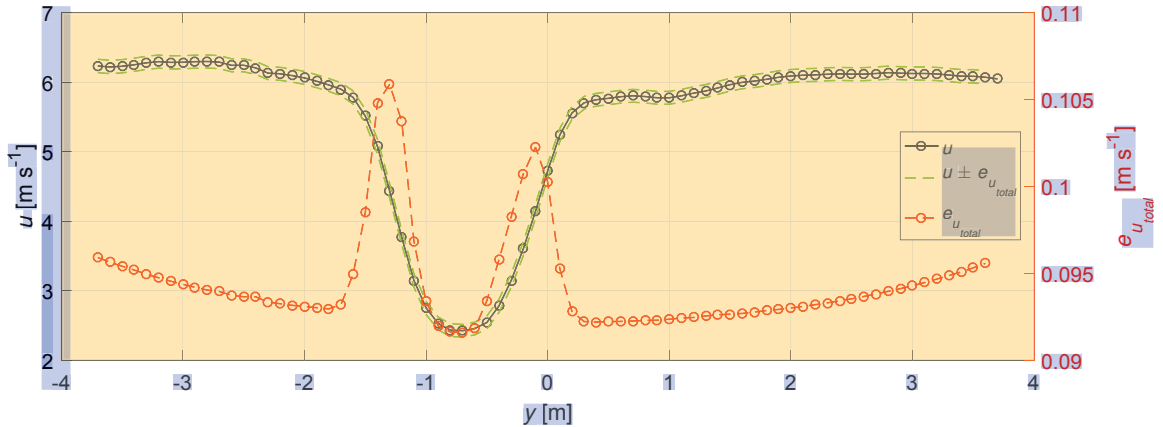

Figure 27. Average wake profile cross-section at a $2D$ downstream distance ($x = 2.2$ m) from the first turbine, with the total error indicated.

To get a better feeling for the magnitude of the additional error caused by the wake boundary gradients, Fig. 27 shows a wake profile at $2D$ downstream distance from turbine one, extracted from Fig. 26. Relative to the actual wake profile, the error bounds cannot be distinguished easily, but when observing the total error $e_{u_{total}}$ separately, an increase of up to 15% with

20 respect to the error e_u can be noticed. This value will increase further when performing the same analysis further downstream.

16

This confirms that one has to be careful with lidar measurements in wind fields containing large gradients, even if the systems are known to have a high pointing accuracy.

4   Conclusions

A first measurement campaign with short-range synchronised WindScanner lidar measurements in a wind tunnel demonstrated
that this technology can be used to measure both the wind tunnel mean flow and turbulence as well as wake profiles of scaled
wind turbines. Validation was performed by comparing the lidar measurements with hot-wire probes, which yielded goodness
of fit coefficients of 0.969 and 0.902 for the 1 Hz averaged u- and v-components of the wind speed, respectively. A downside
is that the lidar systems cannot resolve the smallest turbulence scales, due to the finite measurement probe volumes which
are significantly larger than those of the hot-wire probes. The true turbulence resolution the lidars provide is lower than their
sampling frequency of 390 Hz, in this case even lower than 22 Hz. An extensive uncertainty analysis showed that increased
errors occur in regions with steep spatial velocity gradients. However, lidar as a remote sensing application has the significant
benefit that it does not influence the flow by its presence, contrary to the hot-wire probes, which have to be mounted on a
beam structure that potentially disturbs the flow. Also, the WindScanner technology enables scanning and mapping of entire
two-dimensional horizontal and vertical wind fields within seconds to minutes. It is therefore our conclusion that scanning
wind lidars have significant potential for future wind tunnel measurement applications.

References

Banta, R. M., Pichugina, Y. L., Brewer, W. A., Lundquist, J. K., Kelley, N. D., Sandberg, S. P., Alvarez-II, R. J., Hardesty, R. M., and Weickmann, A. M.: 3D Volumetric Analysis of Wind Turbine Wake Properties in the Atmosphere Using High-Resolution Doppler Lidar, J. Atmos. Oceanic Technol., 32, 904–914, doi:10.1175/JTECH-D-14-00078.1, 2015.

5   Bottasso, C. L., Campagnolo, F., and Petrović, V.: Wind Tunnel Testing of Scaled Wind Turbine Models: Beyond Aerodynamics, Journal of Wind Engineering and Industrial Aerodynamics, 127, 11–28, doi:10.1016/j.jweia.2014.01.009, 2014.

Campagnolo, F., Petrović, V., , Bottasso, C. L., and Croce, A.: Wind Tunnel Testing of Wake Control Strategies, Proceedings of the American Control Conference, pp. 513–518, doi:10.1109/ACC.2016.7524965, 2016a.

Campagnolo, F., Petrović, V., Nanos, E. M., Tan, C., Bottasso, C. L., Paek, I., Kim, H., and Kim, K.: Wind Tunnel Testing of Power

10   Maximization Control Strategies Applied to a Multi-Turbine Floating Wind Power Platform, Proceedings of the International Offshore and Polar Engineering Conference, pp. 309–316, 2016b.

Campagnolo, F., Petrović, V., Schreiber, J., Nanos, E. M., Croce, A., and Bottasso, C. L.: Wind Tunnel Testing of a Closed-Loop Wake Deflection Controller for Wind Farm Power Maximization, Journal of Physics: Conference Series, 753, doi:10.1088/1742-6596/753/3/032006, 2016c.

15   Iungo, G. V.: Experimental Characterization of Wind Turbine Wakes: Wind Tunnel Tests and Wind Lidar Measurements, J. Wind Eng. Ind. Aerodyn., 149, 35–39, doi:10.1016/j.jweia.2015.11.009, 2016.

Iungo, G. V. and Porté-Agel, F.: Volumetric Lidar Scanning of Wind Turbine Wakes under Convective and Neutral Atmospheric Stability Regimes, J. Atmos. Oceanic Technol., 31, 2035–2048, doi:10.1175/JTECH-D-13-00252.1, 2014.

JCGM: Evaluation of Measurement Data: Guide to the Expression of Uncertainty in Measurement, Tech. rep., Joint Committee for Guides

20   in Meteorology, JCGM 201X CD, 2008.

Jørgensen, F. E.: How to Measure Turbulence with Hot-Wire Anemometers - A Practical Guide, Dantec Dynamics, 9040U6151, 2002.

Lignarolo, L. E. M., Ragni, D., Krishnaswami, C., Chen, Q., Ferreira, C. J. S., and van Bussel, G. J. W.: Experimental Analysis of the Wake of a Horizontal-Axis Wind Turbine Model, Renewable Energy, 70, 31–46, doi:0.1016/j.renene.2014.01.020, 2014.

Mikkelsen, T.: About WindScanner.eu, Official Webpage, http://www.windscanner.eu/About-WindScanner, Accessed: 1/6/2016, 2012.

25   Pedersen, A. T., Montes, B. F., Pedersen, J. E., Harris, M., and Mikkelsen, T.: Demonstration of Short-Range Wind Lidar in a High-Performance Wind Tunnel, Proceedings of EWEA 2012, 2012.

Rockel, S., Camp, E., Schmidt, J., Peinke, J., Cal, R. B., and Hölling, M.: Experimental Study on Influence of Pitch Motion on the Wake of a Floating Wind Turbine Model, Energies, 7, 1954–1985, doi:10.3390/en7041954, 2014.

Sathe, A. and Mann, J.: A Review of Turbulence Measurements Using Ground-Based Wind Lidars, Atmos. Meas. Tech., 6, 3147–3167,

30   doi:10.5194/amt-6-3147-2013, 2013.

Simley, E., Angelou, N., Mikkelsen, T., Sjöholm, M., Mann, J., and Pao, L. Y.: Characterization of Wind Velocities in the Upstream Induction Zone of a Wind Turbine Using Scanning Continuous-Wave Lidars, Journal of Renewable and Sustainable Energy, 8, doi:10.1063/1.4940025, 2016.

Sjöholm, M., Mikkelsen, T., Mann, J., Enevoldsen, K., and Courtney, M.: Spatial Averaging Effects of Turbulence Measured by a Continuous-

35   Wave Coherent Lidar, Meteorologische Zeitschrift, 18, doi:10.1127/0941-2948/2009/0379, 2009.

Stawiarski, C., Träumner, K., Knigge, C., and Calhoun, R.: Scopes and Challenges of Dual-Doppler Lidar Wind Measurements - An Error Analysis, J. Atmos. Oceanic Technol., 30, 2044–2064, doi:10.1175/JTECH-D-12-00244.1, 2013.

Taylor, G. I.: The Spectrum of Turbulence, Proc. Roy. Soc. London, 164, 476–490, 1938.

van Dooren, M. F., Trabucchi, D., and Kühn, M.: A Methodology for the Reconstruction of 2D Horizontal Wind Fields of Wind Turbine Wakes Based on Dual-Doppler Lidar Measurements, Remote Sensing, 8, doi:10.3390/rs8100809, 2016.

Wagner, R., Vignaroli, A., Angelou, N., Sathe, A., Forsting, A. R. M., M, Sjöholm, and Mikkelsen, T.: Measurement of Turbine Inflow with a 3D WindScanner System and a SpinnerLidar, in: DEWEK 2015, Bremen, 2015.

Zasso, A., Giappino, S., Muggiasca, S., and Rosa, L.: Optimization of the Boundary Layer Characteristics Simulated at Politecnico di Milano Boundary Layer Wind Tunnel in a Wide Scale Ratio Ranges, Tech. rep., Dipartimento di Meccanica - Politecnico di Milano, 2005.

5